The tight correlation of CCH, and c-C3H2 in diffuse and translucent clouds

Maryvonne Gerin, M. Kazmierczak, M. Jastrzebska, Edith Falgarone, Pierre Hily-Blant, Benjamin Godard, Massimo de Luca

A&A 525, A116 (2011)
DOI: 10.1051/0004-6361/201015050

Astronomy & Astrophysics

The tight correlation of CCH and c-C_3H_2 in diffuse and translucent clouds⋆

M. Gerin[1], M. Kaźmierczak[2], M. Jastrzebska[3], E. Falgarone[1], P. Hily-Blant[4], B. Godard[1], and M. De Luca[1]

[1] LERMA, UMR 8112 du CNRS, Observatoire de Paris, École Normale Supérieure, UPMC & UCP, France
e-mail: [maryvonne.gerin;edith.falgarone;benjamin.godard;massimo.de.luca]@lra.ens.fr
[2] Centre for Astronomy, Nicolaus Copernicus University, Gagarina 11, 87-100 Toruń, Poland
e-mail: maja.kazmierczak@gmail.com
[3] Astronomical Observatory of the Jagiellonian University, Orla 171, Kraków, Poland
e-mail: kulczak@oa.uj.edu.pl
[4] Laboratoire d'Astrophysique de Grenoble, Université Joseph Fourier and CNRS UMR 5571, Observatoire de Grenoble, France
e-mail: pierre.hily-blant@obs.ujf-grenoble.fr

Received 26 May 2010 / Accepted 27 September 2010

ABSTRACT

Using the IRAM 30 m telescope we observed molecular absorption lines from CCH and c-C_3H_2 produced by diffuse and translucent clouds along the lines of sight towards massive star forming regions. The same sources are surveyed with Herschel/HIFI as part of the PRISMAS guaranteed time program, for molecular absorption lines due to hydrides and carbon clusters. The background sources are massive star-forming regions ($G34.3+0.1$, $G10.62-0.39$, $W51$, $W49N$) and SgrA*. The line profiles of the CCH and c-C_3H_2 are strikingly similar for all lines of sight, showing that the ratio of the opacities of the probed transitions, ($J_{K_a,K_c} = 2_{1,2}-1_{0,1}$) for c-$C_3H_2$ and ($J = 1-0, F = 5/2-3/2$) for CCH, is nearly constant along all lines of sight, at $\tau_{\rm CCH} \sim 1.8 \times \tau_{\rm c\text{-}C_3H_2}$. As a consequence, the ratio of the column densities of CCH and c-C_3H_2 is nearly constant and similar to the value derived earlier for diffuse clouds detected along lines of sight towards extragalactic continuum sources, $N({\rm CCH}) = (28 \pm 1.4) N({\rm c\text{-}C_3H_2})$ (Lucas & Liszt 2000, A&A, 358, 1069). PDR models are able to reproduce the observed CCH column densities for the range of physical conditions appropriate for the absorbing matter ($n = 100-3000$ cm^{-3}; $A_V = 1-5$ mag) but can neither fit the observed c-C_3H_2 column densities nor the tight correlation between CCH and c-C_3H_2.

Key words. ISM: clouds – ISM: molecules

1. Introduction

Small carbon containing molecules, with a total of about 1 to 3 carbon atoms, have several interesting properties: they are ubiquitous in the interstellar medium, they are key actors in the formation of long carbon chains and other hydrocarbons, and they are involved in photo-fragmentation process of larger species like PAHs. Of particular interest is the sputtering of carbonaceous nanoparticules, which form a likely source for the high abundance of hydrocarbon molecules detected in the ISM (Pety et al. 2005). It is widely believed that carbon-chain or ring species with more atoms than species detected by radio telescopes might be the candidates for the diffuse interstellar bands (Douglas 1977; Herbig 1975; Herbig 1995). Laboratory studies of the fragmentation process of PAHs have provided further support to this conjecture (Tielens 2008; Useli-Bacchitta & Joblin 2007), but no definitive proof yet. The carbon chemistry is particularly complex. It is initiated in the gas phase by the slow radiative association of ionized carbon with molecular hydrogen leading to CH_2^+ since the direct formation of CH^+ has a high endothermicity of over 4000 K (see the discussion in Godard et al. 2009, and references therein). CH_2^+ then rapidly reacts with H_2, leading to CH_3^+ which acts as the seed for most of the interstellar hydrocarbons (e.g. CH, C_2H_2), as well as the carbon clusters C_2 and C_3. Comparison of carbon clusters and carbon hydrides abundances is therefore an excellent test of the chemical paths to the carbon chemistry and, more generally, to the buildup of molecular complexity in the ISM.

The interstellar ethynyl radical (CCH) was discovered in 1974 by Tucker et al. (1974). It was identified by its radio-astronomical spectra, with the help of its four intense hyperfine components, before laboratory spectroscopy of gaseous CCH was performed. In the interstellar medium, CCH is thought to result from the photodissociation of acetylene (C_2H_2) and from the dissociative recombination of $C_2H_2^+$ and $C_2H_3^+$ (Mul & McGowan 1980). The neutral-neutral reaction between C and CH_2 also contributes to forming CCH especially in moderately shielded regions. This route has been confirmed by the recent measurements of Sakai et al. (2010), who obtained different abundances for the two isotopologues $C^{13}CH$ and ^{13}CCH. Since the two carbon atoms play equivalent roles in the photodissociation of acetylene and in the dissociative recombination of $C_2H_2^+$ and $C_2H_3^+$, the reaction between C and CH_2 is the sole CCH formation mechanism that can produce such a difference in the $C^{13}CH$ and ^{13}CCH abundances because the two carbon atoms have different origins.

Cyclopropenylidene (c-C_3H_2) is the first hydrocarbon ring detected in space. It was reported by Thaddeus et al. (1985); c-C_3H_2 lines were detected as early as 1981 (Thaddeus et al.) but

⋆ Based on observations obtained with the IRAM 30 m telescope.

Table 1. Characteristics of the observed sources.

Object	RA(J2000)	Dec(J2000)	D [kpc]	$V_{\rm LSR}$ [km s^{-1}]	$T_{\rm c}$ [K]	$V_{\rm abs}{}^{a}$ [km s^{-1}]
G34.3+0.1	18 53 18.7	+01 14 58	3.8	57	1.2	6–66
G10.62-0.39(W31C)	18 10 28.7	–19 55 50	4.8	–3	1.0	10–50
W51[b]	19 23 43.9	+14 30 30.5	7.0	55	1.0	2–70
W49N	19 10 13.2	+09 06 12	11.5	7	1.8	14–74
Sgr A*	17 45 51.7	–28 59 08.7	8.6	50	1.5	−30–80

Notes. [(a)] Velocity range of the absorption features. [(b)] This position lies between W51-E1 and W51-E2.

Table 2. Spectroscopic parameters for the observed species.

Molecule	Freq. [GHz]*	$E_{\rm low}$[cm^{-1}]	Transition	A [s^{-1}]	$I_{\rm rel}$	Ref.
CCH, ($N_{J,F}$)	87.284105	0.0015	$1_{3/2,1}-0_{1/2,1}$	2.59×10^{-7}	0.1	CDMS
	87.316898	0.0015	$1_{3/2,2}-0_{1/2,1}$	1.53×10^{-6}	1.0	CDMS
	87.328585	0.0000	$1_{3/2,1}-0_{1/2,0}$	1.27×10^{-6}	0.5	CDMS
	87.401989	0.0015	$1_{1/2,1}-0_{1/2,1}$	1.27×10^{-6}	0.5	CDMS
	87.407165	0.0015	$1_{1/2,0}-0_{1/2,1}$	1.53×10^{-6}	0.2	CDMS
	87.446470	0.0000	$1_{1/2,1}-0_{1/2,0}$	2.61×10^{-7}	0.1	CDMS
c-C_3H_2, (J_{K_a,K_c})	85.338893	1.6332	$2_{1,2}-1_{0,1}$	2.55×10^{-5}		JPL
HCS^+, (J)	85.347890	1.4235	2–1	1.11×10^{-5}		CDMS

Notes. [(*)] CCH frequencies derived from Padovani et al. (2009); JPL refers to the JPL spectral line catalog (Pickett et al. 1998); CDMS refers to the Cologne Data Base for Molecular Spectroscopy (Müller et al. 2001, 2005).

were not identified as a cyclopropenylidene until 1985. c-C_3H_2 is also one of the most abundant molecules with 3 carbon atoms in the interstellar medium (Teyssier et al. 2004). Its main gas phase formation route is the dissociative recombination of c-$C_3H_3^+$.

Both CCH and c-C_3H_2 are therefore good probes for hydrocarbons in the diffuse interstellar medium, especially carbon chains and radicals. While the inventory of gas-phase carbon molecules with two or three C-atoms is fairly complete (Marcelino et al. 2007), knowledge of species with more carbon atoms is still fragmentary. Combined measurements of CCH and c-C_3H_2 can shed light on the chemical processes leading to larger hydrocarbons. Lucas & Liszt (2000) show that interstellar absorption features from CCH and c-C_3H_2 are correlated well in the millimeter spectra of extragalactic background radio sources with N(CCH)/N(c-C_3H_2) = 27.7 ± 8. Pety et al. (2005) found a spatial correlation of emission maps of the edge of the Horsehead nebula, with a strong similarity between maps of CCH, c-C_3H_2 and C_4H, but with differences in the mean abundance ratios: N(CCH)/N(c-C_3H_2) = ∼ 12 and N(CCH)/N(C_4H) = ∼ 7.

In this paper, we present new absorption spectra, sampling the diffuse and translucent matter in the Galactic Plane, along lines of sight towards bright millimeter continuum sources. The data set belongs to complementary absorption spectroscopy data obtained with the IRAM-30 m telescope towards the targets of the PRISMAS (PRobing InterStellar Molecules with Absorption line Studies) Herschel key program. This project aims at probing the first steps of the oxygen, carbon and nitrogen chemistry in the diffuse interstellar medium. Extensive spectroscopic studies of key interstellar molecules not easily accessible at other wavelengths, namely hydrides and carbon clusters, are currently performed by Herschel/HIFI. The target sources have been selected as strong (sub)millimeter continuum sources, with known intervening interstellar features along the lines of sight. The same sources can be observed at millimeter wavelengths, although the continuum emission is produced by the embedded HII regions rather than by dust. While a first set of observations, covering HCO^+, HCN, HNC and CN spectra, has been presented by Godard et al. (2010), the data relative to the hydrocarbon chemistry are presented in this paper. The analyzed objects are listed in Table 1. Table 1 also lists their distances from Fish et al. (2003).

The next section describes the IRAM-30 m observations. The results are presented in Sect. 3; a comparison with PDR models is given in Sect. 4, while Sect. 5 presents the conclusions.

2. Observations

2.1. Data analysis and processing

The observations were performed with the IRAM-30 m telescope in 2006 August and December. We used the A100 and B100 receivers, simultaneously with either the A230, B230 or the C150, D150 receivers. All receivers were operated in single side band mode, with a rejection of the image side band better than a factor of 20 (13dB). The observations were performed with the wobbling secondary reflector to obtain flat and stable baselines, and an accurate measurement of the 3 mm radio continuum intensity. The wobbler throw was 240 arcsec and the switching rate 0.5 Hz. The weather conditions were averaged with 5–10 mm of water vapor in August 2006 and less than 3 mm in December 2006. The pointing was checked on nearby planets and continuum sources, and was found accurate within 5 arcsec. The lines were analyzed with the flexible, high spectral resolution backend VESPA, tuned to a spectral resolution of 40 kHz (∼0.13 km s^{-1}), and spectral bandpass of 120 MHz covering a velocity range of ∼400 km s^{-1}. We also used the 1 MHz filterbank to obtain broad band spectra. We searched for the ground state transition of CCH at 87.316 GHz and the $2_{1,2}-1_{0,1}$

transition of ortho c-C_3H_2 at 85.338 GHz. The $J = 2$–1 line of HCS^+ was observed simultaneously with c-C_3H_2 as their frequencies are very close (the velocity shift is -31.6 km s^{-1}). The spectroscopic parameters of the observed molecular transitions are listed in Table 2. The IRAM-30 m spectra are shown in Fig. 1.

The data processing was done with the GILDAS[1] softwares (e.g. Pety 2005). The IRAM-30 m data were first calibrated to the T_A^* scale using the chopper wheel method (Penzias & Burrus 1973), and finally converted to main beam temperatures T_{mb} using the forward and main beam efficiencies F_{eff} and B_{eff} appropriate for 85 and 87 GHz: $F_{eff} = 0.95$ and $B_{eff} = 0.75$. The resulting temperature accuracy is ∼10%, as checked by the variation of the intensity of the strong CCH emission lines in the spectra between different days.

The spectra show strong emission lines associated with the massive cores surrounding the compact HII regions, together with absorption lines from the foreground matter along the line of sight. In the massive star forming regions, the continuum emission is mainly free-free emission while we detect the non thermal millimeter continuum emission from SgrA*. The continuum intensities are listed in Table 1. Except for SgrA*, emission lines of CCH ($1_{3/2,2}$–$0_{1/2,1}$) at 87.316 GHz, CCH ($1_{3/2,1}$–$0_{1/2,0}$) at 87.328 GHz, and c-C_3H_2 $2_{1,2}$–$1_{0,1}$ at 85.339 GHz are detected at the velocities of the background sources. The $J = 2$–1 line of HCS^+ at 85.347 GHz i.e. -31.6 km s^{-1} relative to the c-C_3H_2 ($2_{1,2}$–$1_{0,1}$) line is also detected in all sources. Emission lines have close to Gaussian profiles towards G10.6–0.39, G34.3+0.15 and W51, while they are clearly double peaked towards W49N, a feature also seen in other molecular lines Williams et al. (2004). In this paper, we analyse the absorption produced by the foreground matter along the line of sight and will not comment further on the emission spectra.

The continuum intensity T_c was measured by fitting flat baselines to the spectra. The spectra were then normalized by dividing them by T_c. The parameters (central opacity τ, velocity V and line width δV) of the detected absorption features were derived by fitting Gaussian absorption profiles to the normalized spectra. They are defined as:

$$T_{mb} = T_c e^{-\tau} \quad (1)$$

and hence:

$$\tau = -\ln\left(\frac{T_{mb}}{T_c}\right). \quad (2)$$

The CCH and c-C_3H_2 absorption profiles are strikingly similar, with narrow components superposed with broad and shallow features. Given the complexity of these profiles, we did not attempt to fit them entirely but preferred to restrict the analysis to the narrow features that have Gaussian profiles and are easily identified in the spectra (Fig. 2). We started with the CCH data that have the best S/N ratio. As the main CCH hyperfine components is separated from the nearest satellite line by ∼11.7 MHz ∼40 km s^{-1}, the absorptions caused by these components do not overlap in most cases. We used the detection of the main and satellite lines to check the quality of the fit of the line parameters. Once the fit of the CCH spectra was satisfactory, and in order to decrease the number of free parameters in the fit, we used the centroid velocities of the CCH velocity components as constraints for the fit of the c-C_3H_2 line profiles. The high spectral resolution used in this study allowed us to separate velocity

[1] See http://www.iram.fr/IRAMFR/GILDAS

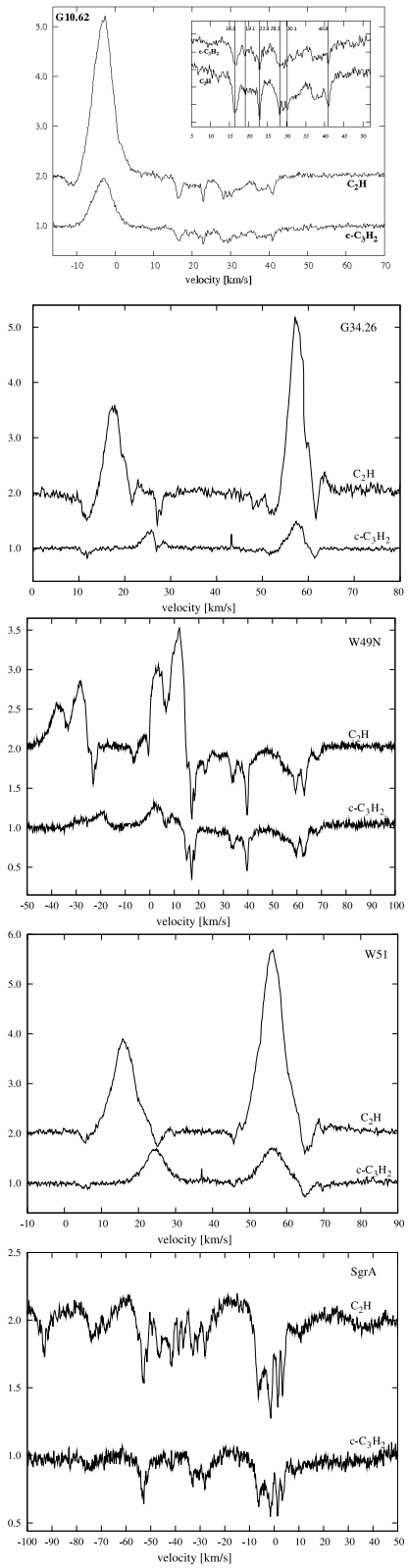

Fig. 1. Spectra obtained with the IRAM-30 m telescope. The velocity scale is given relative to the Local Standard of Rest (LSR). The spectra have been normalized by dividing the individual measurements by the source continuum intensities. The CCH spectra have been offset for clarity. Except for G10.6, the two strongest CCH hyperfine components at 87.317 and 87.329 GHz are shown. The emission line shifted by -31.6 km s^{-1} from c-C_3H_2 is the HCS^+ $J = 2$–1 transition at 85.347 GHz. An inset showing the velocities of the absorption features is presented for G10.62.

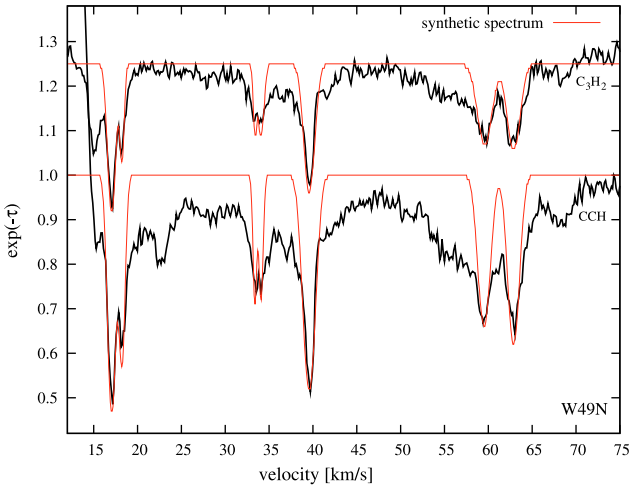

Fig. 2. The multiple velocity component fit overlayed on a zoom of the W49N data. Broad absorption is clearly detected in CCH and c-C_3H_2 in the velocity ranges ~30−45 and ~50−70 km s^{-1} corresponding to the Sagittarius and Scutum spiral arms.

components which were blended in previous studies (Madden et al. 1989; Cernicharo et al. 1999; Cox et al. 1988). The global analysis of the CCH and c-C_3H_2 absorption profiles (Fig. 4) shows that the broad absorption features have similar properties to the narrow lines.

Although the available HI data (Fish et al. 2003; Koo 1997) have a lower spectral resolution than the data presented here, there is a generally good correspondence of the velocity ranges where absorption is detected in HI and in other molecules such as HCO^+ or CCH. Note however that some HI features seem to have little molecular counterpart while the reverse is never seen. As discussed further in (Godard et al. 2010; Neufeld et al. 2010b), the opacities of the absorption features do not scale with the HI opacities, indicating that the abundances of the different species relative to HI vary among velocity components. The recent *Herschel*-HIFI spectra obtained within the framework of the PRISMAS key programme show more extensive examples of molecular line profiles towards G10.6, W49N and W51 (Falgarone et al. 2010; Gerin et al. 2010a,b; Neufeld et al. 2010a,b; Sonnentrucker et al. 2010; Persson et al. 2010). The Herschel data revealed that absorption features from the molecular ions CH^+, OH^+ and H_2O^+, and from the HF molecule are better correlated with HI than those from triatomic molecules such as CCH and HCO^+ (Falgarone et al. 2010; Gerin et al. 2010a; Neufeld et al. 2010a,b; Sonnentrucker et al. 2010).

2.2. Derivation of CCH column densities

We analyzed the main CCH hyperfine component at 87.316 GHz. As shown in Fig. 1, the absorption spectra are not saturated, for all hyperfine components, including the strongest one. Furthermore, the satellite hyperfine components that have lower relative intensities (Table 2) present weaker absorption features than the strongest component. For all sources, the ratio of the opacities of the satellite line at 87.328 GHz divided by the opacity of the main line at 87.317 GHz is equal to 0.5, the ratio of the relative intensities, as expected for unsaturated lines. This shows that the opacity of the absorption features is truly moderate, and does not result from partial coverage of the background source of saturated absorption lines, because in the latter case, we would expect that the relative intensities of the CCH hyperfine components would depart from their theoretical values, that are listed in Table 2. At millimeter wavelengths, the covering factor of the absorbing matter is close to unity.

We derived the molecule column densities using the relation:

$$\begin{aligned} N_{\rm tot} &= Z(T_{\rm ex}) \times N_u \times \frac{e^{\frac{E_u}{kT_{\rm ex}}}}{g_u} \\ &= Z(T_{\rm ex}) \frac{8\pi\nu^3}{c^3} \frac{e^{E_u/kT_{\rm ex}}}{(g_u A_{\rm ul})(e^{h\nu/kT_{\rm ex}} - 1)} \int \tau \cdot {\rm d}v \end{aligned} \quad (3)$$

where $Z(T_{\rm ex})$ is the partition function computed at the excitation temperature $T_{\rm ex}$, $N_{\rm tot}$ and N_u are the total column density and the column density in the upper state of the transition respectively, g_u is the statistical weight of the upper level, $A_{\rm ul}$ is the Einstein coefficient for spontaneous emission, ν is the line frequency and $\int \tau \cdot {\rm d}v$ is the line opacity integrated over the line profile. For molecules with hyperfine structure like CCH it can be easier to compute the column density without taking the hyperfine structure into account, provided that the correct line opacity, i.e. the sum of the opacities of all hyperfine components, is used. Following the latter approach and assuming that the excitation temperature is equal to the CMB, 2.73 K, i.e. collisional excitation is negligible because of the low gas density and moderate kinetic temperature, this leads to the relation given by Lucas & Liszt (2000):

$$\begin{aligned} N(C_2H) &= 2.71 \times 10^{13} \cdot 2.4 \cdot \int \tau {\rm d}v \ [{\rm cm}^{-2}] \\ &= (2.4 \cdot 2.71 \cdot 1.065) \times 10^{13} \cdot fwhm \cdot \tau [{\rm cm}^{-2}] \end{aligned} \quad (4)$$

where $fwhm$ is the line full width at half maximum in km s^{-1} and τ is the opacity of the main hyperfine component ($1_{3/2,2}$–$0_{1/2,1}$ at 87.316 GHz). The factor 2.4 corrects for the opacities of the satellite lines because Lucas & Liszt (2000) quoted this formula differently, with the sum of the opacities of all hyperfine components rather the opacity of the main component ($1_{3/2,2}$–$0_{1/2,1}$) we are using. For a Gaussian line profile the integrated line opacity is proportional to the product of the line width at half maximum $fwhm$ and central opacity τ. The factor is very close to unity, and can be written as $\sqrt{\frac{\pi}{4ln(2)}} \simeq 1.065$.

The hypothesis of negligible collisional excitation has been confirmed by the multi transition analysis of the HCO^+ profiles (Godard et al. 2010) and by additional, non LTE, statistical equilibrium calculations performed with the RADEX software (van der Tak et al. 2007, Black private communication). We checked that the excitation temperature of the observed CCH transition stays below 3 K, for most of the domain of physical conditions applicable to the line of sight clouds: the absorption features are formed in moderately dense gas: $n(H_2) = 100$–3000 cm^{-3} (Plume et al. 2004; Vastel et al. 2000; Godard et al. 2010). These analyses have shown that, with such physical conditions, the collisional excitation of polar molecules is rather ineffective, and the excitation temperature remains close to the cosmic background temperature. The excitation temperature starts to depart significantly from the cosmic background temperature at the highest densities ($n(H_2) > 3000$ cm^{-3}), but never rises above 5 K. Therefore, we can confidently derive the molecular column densities assuming that the excitation temperature is equal to the CMB.

2.3. Derivation of c-C_3H_2 column densities

Absorption in the strong $2_{12}-1_{01}$ transition of ortho c-C_3H_2 at 85.338 GHz is detected in all sources. The similarity of the spectra to those of CCH (Fig. 4) suggests that the absorption features are not saturated and that we can derive accurate column densities from the measured line opacities.

The c-C_3H_2 column densities were derived from the relation of Lucas & Liszt (2000):

$$N(c-C_3H_2) = 4.36 \cdot 10^{12} \cdot fwhm \cdot \tau \ [\mathrm{cm}^{-2}]. \quad (5)$$

As for CCH, this equation is based on the assumption of no collisional excitation. The results are listed in Table 3.

2.4. HCS^+

The HCS^+ $J = 2-1$ transition at 85.347 GHz is detected in emission, shifted by -31.6 km s^{-1} from c-C_3H_2 line at 85.338 GHz, but does not show any detectable absorption down to the noise level. Assuming $T_{ex} = 2.73$ K, we derived an upper limit of $\tau \leq 0.1$ and $N(HCS^+) = 9.27 \times 10^{12} fwhm \cdot \tau < 9.3 \times 10^{11}$ cm^{-2} for a line width of 1 km s^{-1}.

3. Results

Table 3 summarizes the derived CCH and c-C_3H_2 line parameters and column densities. For each velocity component, the full line width at half maximum ($fwhm$), the opacity (τ) and column density (N) are given. The distance to the different velocity components is also listed. It is derived assuming a flat rotation curve using: $\theta_0 = 220$ km s^{-1} and $R_0 = 8.5$ kpc as recommended by the IAU (Kerr & Lynden-Bell 1986).

3.1. Analysis of CCH and c-C_3H_2 line profiles

As shown in Fig. 1, the CCH and c-C_3H_2 spectra are strikingly similar. To be more quantitative, we show in Figs. 3a and 3b comparisons of the line full width at half maximum $fwhm$ and central opacity τ for the analyzed absorption features. The correlation coefficients for the derived central opacity and line width are 0.85 and 0.89 respectively, showing that these variable are strongly correlated. Figure 4 presents direct comparisons of the line profiles expressed in opacity units, for the entire velocity ranges where absorption is detected. The symbols indicate the different sources. The five sources share the same mean relation.

We therefore conclude that the data are consistent with the hypothesis that the CCH and c-C_3H_2 absorption features have identical line widths, and that their line opacities are proportional with $\tau(\mathrm{CCH}) = 1.8 \pm 0.2 \cdot \tau(\text{c-}C_3H_2)$, where τ(CCH) refers to the opacity of the main hyperfine component. This conclusion is based on the sole analysis of the line profiles and does not depend on any assumption on the line formation mechanism, nor on the decomposition method of the complex profiles into individual velocity components.

3.2. Comparison of CCH and c-C_3H_2 column densities

As expected from the tight relationship of the CCH and c-C_3H_2 line opacities and line widths, column densities of CCH and c-C_3H_2 are linearly correlated, with a correlation coefficient of 0.88. Fig. 3c) illustrates this correlation. It is interesting to note that we obtained a very similar relationship between the CCH and c-C_3H_2 column densities as in the study of local diffuse clouds performed by Lucas & Liszt (2000): $N(\mathrm{CCH})/N(\text{c-}C_3H_2) = 28.2 \pm 1.4$ while they found $N(\mathrm{CCH})/N(CthHtw) = 27.7 \pm 8$.

4. Chemistry

We used the Meudon-PDR code (Le Petit et al. 2006; Goicoechea & Le Bourlot 2007; González-García et al. 2008) to investigate the production mechanisms of CCH and c-C_3H_2. The cold gas is modeled as a slab of either constant density or constant pressure, illuminated by the average interstellar radiation field on both sides. The code assumes that the chemistry has reached steady state, and computes the thermal equilibrium by balancing the cooling and heating rates at each point in the slab. The main input parameters are listed in Table 4. We used the default values for the elemental abundances, extinction curve and cosmic ray ionization rate ζ as discussed by e.g. (Le Petit et al. 2006). The physical conditions of the matter giving rise to the absorption features are fairly well known from previous works: the gas densities and total extinction across each absorption feature are low to moderate (Godard et al. 2010; Gerin et al. 2010b). We therefore chose to run models with constant gas densities ranging from 100 to 1000 cm^{-3}, and added two models with constant pressure. We show models with total hydrogen densities of $n(\mathrm{H}) = 100$, 250, 500, 750 and 1000 cm^{-3}, gas pressures of 3500 and 10^4 K cm^{-3}, and total extinction across the slab of $A_V = 1, 3$, and 5 mag. For all models, the radiation field has been set to the mean interstellar radiation field in the solar neighborhood $G_0 = 1$. We briefly explored the role of the cosmic ray ionization rate ζ, by running models with $\zeta = 10^{-16}$ s^{-1} and 2×10^{-16} s^{-1} for $n_{\mathrm{H}} = 500$ cm^{-3}, following the recent H_3^+ observations summarized in Indriolo et al. (2007) that suggest that ζ may be higher in the diffuse interstellar medium than in the dense gas. Table 5 lists the model predictions for the column densities across the slab.

Figure 5 shows the predicted column densities of C^+, C, CO, CH, CCH and c-C_3H_2 across the slab for the models. The constant density models are plotted with squares, while the constant pressure models are indicated by stars. Models with $A_V = 3$ mag are shown with black symbols and full lines, while we show models with $A_V = 5$ mag with white symbols and dotted lines and models with $A_V = 1$ mag with crosses. To ease the comparison, we scaled all model predictions to $A_V = 3$ mag. The predicted column densities of the $A_V = 5$ mag cases are therefore multiplied by 0.6, while the predicted column densities of the $A_V = 1$ mag are multiplied by 3. The constant pressure models are plotted using the maximum density as abscissa.

In these models, CCH reaches total column densities ranging from comparable to somewhat higher than what we measured, while the c-C_3H_2 column densities remain lower than observed. The abundance ratio ranges from ~160 to >400, the highest value being obtained for the lowest density models. The spatial distribution of the CCH and c-C_3H_2 abundances is also different: while CCH is present as soon as $A_v > 0.5$ mag or even at lower extinctions for the $n = 1000$ cm^{-3} models, c-C_3H_2 is confined in the inner core of the slab with $A_v > 1$ mag. The behaviors of the predicted CCH and c-C_3H_2 column densities with the slab density and total extinction also differ. Except for the densities in the $A_V = 1$ mag case, the predicted CCH column density is independent of the model density and scales with A_V. On the contrary, the highest c-C_3H_2 column densities are obtained for the models with highest extinction, and at a given extinction for the highest density.

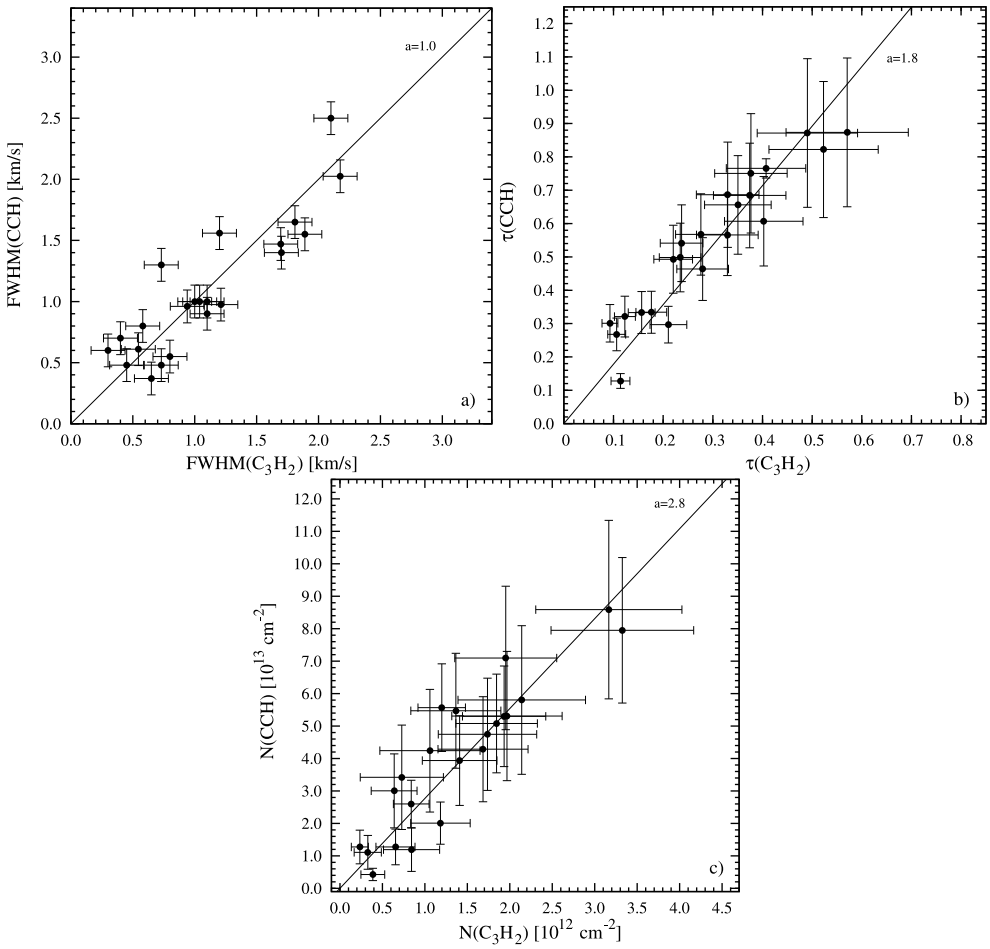

Fig. 3. a) Comparison of the Full Width at Half Maximum (*FWHM*) of the velocity components identified in the CCH and c-C_3H_2 line profiles. The straight line indicates a slope of 1.
b) Comparison of the line center opacities τ of the observed CCH and c-C_3H_2 lines. For CCH the opacity of the strongest hyperfine component at 87.317 GHz is plotted. The line shows the mean relation with a slope of $a = 1.8$.
c) Comparison of the column densities of CCH and c-C_3H_2. The line shows a slope of 2.8, corresponding to the relation obtained by Lucas & Liszt (2000) towards diffuse clouds at high Galactic latitude, $N(\mathrm{CCH}) \sim 28\ N(\mathrm{c\text{-}C_3H_2})$. We get a similar result, $N(\mathrm{CCH})/N(\mathrm{c\text{-}C_3H_2}) = 28.2 \pm 1.4$.

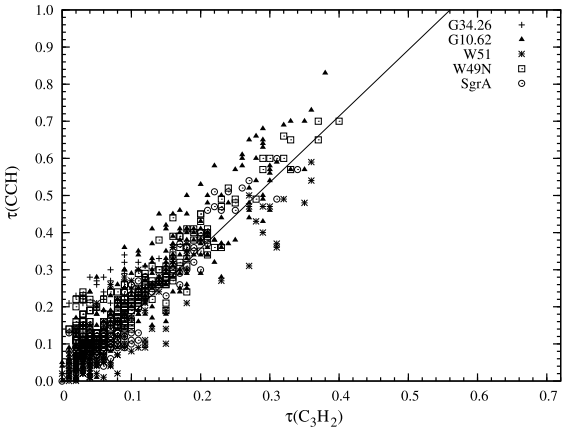

Fig. 4. Comparison of the opacities of the individual velocity channels for the CCH ($1_{5/2,5/2}-0_{3/2,3/2}$) and c-C_3H_2 ($2_{1,2}-1_{0,1}$) lines. The straight line shows the mean ratio $\tau(\mathrm{CCH})/\tau(\mathrm{c\text{-}C_3H_2}) = 1.8$. The typical error on the opacities in each velocity channel is about ~0.1.

All models predict a high molecular fraction $f(H_2) = \frac{2N(H_2)}{N(H)+2N(H_2)} > 0.9$, since atomic hydrogen is only dominant over molecular hydrogen in the most external layers ($A_V < 0.1$ mag) of the modeled clouds. The molecular fraction is not known for all lines of sight. For G10.6–0.4 and W49N, it is possible to estimate this parameter from the comparison of the total extinction along the line of sight with the observed HI absorption. The average molecular fraction is 0.4–0.6 (Godard et al. 2010; Neufeld et al. 2010a) but the detailed comparison of the HI and molecular absorption profiles reveals that a variety of conditions is present, from very diffuse phases with mostly atomic gas to mostly molecular gas (Neufeld et al. 2010b).

Figure 6 presents abundances relative to H_2 derived from the PDR models in the sampled parameter space. Because both CH and CCH scale well with the extinction across the slab, their abundances relative to H_2 show little variation with the gas density. The PDR models reproduce the well known correlation of CH with molecular hydrogen (Sheffer et al. 2008, and references therein). The predicted abundances are slightly higher than the mean CH abundance derived from visible absorption spectroscopy: we deduce $[\mathrm{CH}] \sim 1.3 \pm 0.2 \times 10^{-7}$ and $[\mathrm{CCH}] \sim 7.0 \pm 1.5 \times 10^{-8}$ relative to the H_2 column density, while Sheffer et al. (2008) derived $[\mathrm{CH}] = 3.6 \times 10^{-8}$ for diffuse and translucent clouds of somewhat lower total extinctions. It is remarkable that, for both CH and CCH, the variation of their abundance relative to H_2 does not exceed 20% for most of the studied models.

Table 3. Results of measurements for absorption structures of CCH and c-C_3H_2 (the full width at half maximum $fwhm$, the line center opacity τ, the column density N).

Source	CCH			c-C3H2			D [kpc]
v[km s]	$fwhm$[km s^{-1}]	τ	N[10^{13} cm^{-2}]	$fwhm$[km s^{-1}]	τ	N[10^{12} cm^{-2}]	
G34.26							
51.95	2.50 ± 0.13	0.32 ± 0.06	5.57 ± 1.35	2.10 ± 0.13	0.12 ± 0.02	1.20 ± 0.28	3.4
61.30	0.98 ± 0.13	0.30 ± 0.06	2.01 ± 0.65	1.21 ± 0.13	0.21 ± 0.04	1.18 ± 0.35	4.0
G10.62							
16.55	1.65 ± 0.13	0.75 ± 0.18	8.59 ± 2.75	1.81 ± 0.13	0.38 ± 0.07	3.17 ± 0.86	2.5
19.08	0.37 ± 0.13	0.46 ± 0.09	1.19 ± 0.67	0.65 ± 0.13	0.28 ± 0.05	0.84 ± 0.33	2.8
22.83	0.96 ± 0.13	0.87 ± 0.22	5.80 ± 2.29	0.94 ± 0.13	0.49 ± 0.10	2.14 ± 0.75	3.2
28.06	0.70 ± 0.13	0.87 ± 0.22	4.24 ± 1.89	0.40 ± 0.13	0.57 ± 0.12	1.06 ± 0.59	3.6
30.20	0.60 ± 0.13	0.82 ± 0.20	3.42 ± 1.61	0.30 ± 0.13	0.52 ± 0.11	0.73 ± 0.49	3.7
40.93	1.30 ± 0.13	0.61 ± 0.13	5.47 ± 1.77	0.73 ± 0.13	0.40 ± 0.08	1.37 ± 0.53	4.4
W51							
5.31	1.40 ± 0.13	0.27 ± 0.05	2.60 ± 0.73	1.70 ± 0.13	0.11 ± 0.02	0.84 ± 0.21	0.4
6.49	0.48 ± 0.13	0.13 ± 0.02	0.43 ± 0.19	0.73 ± 0.13	0.11 ± 0.02	0.39 ± 0.14	0.5
45.59	0.61 ± 0.13	0.30 ± 0.06	1.27 ± 0.52	0.55 ± 0.13	0.09 ± 0.02	0.24 ± 0.10	3.9
65.20	2.03 ± 0.13	0.57 ± 0.12	7.95 ± 2.24	2.18 ± 0.13	0.33 ± 0.06	3.33 ± 0.84	
W49N							
16.94	1.00 ± 0.13	0.77 ± 0.03	5.31 ± 1.99	1.04 ± 0.13	0.41 ± 0.08	1.97 ± 0.65	1.3
18.29	0.80 ± 0.13	0.54 ± 0.12	3.00 ± 1.14	0.58 ± 0.13	0.24 ± 0.04	0.64 ± 0.27	1.3
33.27	0.48 ± 0.13	0.33 ± 0.06	1.11 ± 0.52	0.45 ± 0.13	0.16 ± 0.03	0.33 ± 0.16	2.4
34.07	0.55 ± 0.13	0.33 ± 0.06	1.27 ± 0.55	0.80 ± 0.13	0.18 ± 0.03	0.65 ± 0.23	2.4
39.56	1.56 ± 0.13	0.66 ± 0.15	7.10 ± 2.21	1.20 ± 0.13	0.35 ± 0.07	1.95 ± 0.60	2.8
59.44	1.55 ± 0.13	0.49 ± 0.10	5.30 ± 1.55	1.89 ± 0.13	0.22 ± 0.04	1.93 ± 0.49	4.4
62.84	1.47 ± 0.13	0.50 ± 0.10	5.08 ± 1.52	1.70 ± 0.13	0.23 ± 0.04	1.84 ± 0.48	4.7
Sgr A							
–6.35	0.90 ± 0.13	0.69 ± 0.16	4.29 ± 1.62	1.10 ± 0.13	0.33 ± 0.06	1.68 ± 0.53	8.4
1.4	1.00 ± 0.13	0.68 ± 0.16	4.75 ± 1.73	1.00 ± 0.13	0.37 ± 0.07	1.74 ± 0.58	8.9
3.49	1.00 ± 0.13	0.57 ± 0.12	3.94 ± 1.38	1.10 ± 0.13	0.28 ± 0.05	1.41 ± 0.44	8.6

Table 4. Parameters of the PDR models

Radiation field G_0	1
Helium abundance	0.1
Oxygen abundance	3.2×10^{-4}
Carbon abundance	1.3×10^{-4}
Nitrogen abundance	7.5×10^{-5}
Fe abundance	1.5×10^{-8}
Cosmic ray ionization rate ζ	5×10^{-17} s^{-1}
$R_V = A_V/E(B-V)$	3.1
Gas to Dust ratio	100
Grain size distribution index	3.5
Minimum grain radius	0.003 μm
Maximum grain radius	0.3 μm

The PDR models also predict that the ratio of the CH and CCH abundances is well defined: N(CH)/N(CCH) = 1.8 ± 0.3. This close association of CH and CCH is confirmed when looking at the spatial gradients of the CH and CCH densities in a single slab as the spatial variations of CH and CCH are very similar. This behavior can be understood since these species are closely chemically related. CCH is produced by the photodissociation of acetylene (Roberge et al. 1991) and by the reaction of atomic carbon with CH_2 (Smith et al. 2004; Sakai et al. 2010). The dissociative recombination of molecular ions such as $C_2H_2^+$ and $C_2H_3^+$ also plays a role. CCH is destroyed by photodissociation and by reaction with ionized and atomic carbon, initiating the formation of polyynes. As the carbon chemistry is initiated by the radiative association between C^+ and H_2 producing CH_2^+ (Black & Dalgarno 1973), it is expected that CH scales with H_2. The formation of diatomic hydrocarbons is relatively easy once CH_2^+ is formed because the reactions with C^+ and C are rapid. Hence models predict that CH and CCH reside in the same environment. Furthermore, the predicted CH_2 column densities are similar to those of CH and slightly higher than those of CCH, with a trend with the gas density. CH is more abundant for the low densities, while CH_2 becomes dominant for $n \geq 500$ cm^{-3}.

Within the limited parameter space sampled, we did not find any strong variation of the predicted CCH or CH abundances with the cosmic ray ionization rate ζ. We recovered the known decrease of the CO abundance with increasing ζ (see Table 5 and Fig. 6).

It will be interesting to confirm these model predictions by observing CH along the same lines of sight as CCH. Observations of the ground state rotational lines of CH at 532 and 536 GHz at high spectral resolution are now feasible using the HIFI instrument on board the Herschel Space Observatory. First observations presented by (Gerin et al. 2010b) show a tight association of CH and CCH for a limited source sample. If the trend is confirmed, it will be possible to use CCH as a proxy for molecular hydrogen in diffuse and translucent gas, since CH has been shown to be tightly correlated with the molecular hydrogen (Federman 1982; Liszt & Lucas 2002; Weselak et al. 2004; Sheffer et al. 2008).

On the contrary, the model does not reproduce the observed properties of c-C_3H_2 : i) the predicted column densities are lower than the observed column densities; ii) the predicted column density does not scale with the total extinction across the slab. Moreover, because CCH is present across most of the slab, while c-C_3H_2 is confined to the inner regions, the resulting line profiles are expected to bear the signature of these different environments, with c-C_3H_2 profiles sampling quieter regions with smaller velocity dispersions than CCH. Therefore a loose correlation between the CCH and c-C_3H_2 line profiles would be

Table 5. Column densities N[cm^{-2}] predicted by the PDR models. Models 1–15 and 18–21 are isochoric (constant n_H) models 16 and 17 are isobaric.

Model	A_v[mag]	n_H[cm^{-3}]	$N(H_2)$	$N(H)$	$N(C^+)$	$N(C)$	$N(CO)$	$N(CH)$	$N(C_2H_2)$	$N(CH_2)$	$N(CCH)$	$N(C_3H_2)^*$
1	5	100	4.5E21	3.9E20	7.6E17	3.9E17	7.4E16	6.3E14	1.1E12	4.6E14	3.0E14	8.4E11
2	5	250	4.6E21	1.8E20	5.9E17	4.3E17	1.9E17	6.1E14	1.7E12	5.4E14	3.4E14	1.5E12
3	5	500	4.6E21	1.1E20	4.8E17	4.3E17	3.0E17	5.7E14	1.9E12	5.9E14	3.4E14	1.8E12
4	5	750	4.6E21	8.0E19	4.1E17	4.4E17	3.6E17	5.3E14	2.0E12	6.0E14	3.3E14	1.9E12
5	5	1000	4.6E21	6.6E19	3.7E17	4.4E17	4.0E17	5.0E14	2.0E12	6.0E14	3.3E14	2.0E12
6	3	100	2.7E21	3.1E20	6.6E17	7.5E16	3.5E15	3.2E14	7.5E10	1.7E14	1.1E14	5.8E10
7	3	250	2.7E21	1.5E20	5.7E17	1.5E17	1.8E16	3.9E14	2.8E11	3.0E14	1.8E14	2.2E11
8	3	500	2.8E21	9.2E19	4.7E17	2.0E17	5.3E16	4.1E14	6.4E11	4.1E14	2.3E14	4.9E11
9	3	750	2.8E21	7.0E19	4.1E17	2.2E17	8.9E16	4.1E14	9.4E11	4.6E14	2.5E14	7.3E11
10	3	1000	2.8E21	5.9E19	3.7E17	2.3E17	1.2E17	4.1E14	1.2E12	4.8E14	2.6E14	9.2E11
11	1	100	8.3E20	2.2E20	2.5E17	1.4E15	5.2E13	4.6E13	7.0E08	1.6E13	5.4E12	3.8E08
12	1	250	8.9E20	9.6E19	2.4E17	4.4E15	4.2E13	9.2E13	6.0E09	4.4E13	2.4E13	5.5E09
13	1	500	9.1E20	5.6E19	2.4E17	1.0E16	1.0E14	1.3E14	2.3E10	8.2E13	4.9E13	2.3E10
14	1	750	9.1E20	4.3E19	2.3E17	1.6E16	2.0E14	1.4E14	4.4E10	1.1E14	6.4E13	4.2E10
15	1	1000	9.2E20	3.6E19	2.2E17	2.2E16	3.3E14	1.5E14	6.7E10	1.3E14	7.3E13	6.0E10
model	A_v[mag]	p[K cm^{-3}]	$N(H_2)$	$N(H)$	$N(C^+)$	$N(C)$	$N(CO)$	$N(CH)$	$N(C_2H_2)$	$N(CH_2)$	$N(CCH)$	$N(C_3H_2)^*$
16	5	3500	4.4E21	5.9E20	5.6E17	3.8E17	2.8E17	4.6E14	1.5E12	4.2E14	2.5E14	1.5E12
17	5	10000	4.6E21	1.1E20	3.9E17	3.8E17	4.4E17	4.1E14	1.5E12	4.6E14	2.5E14	1.6E12
model	A_v[mag]	ζ [s^{-1}]	$N(H_2)$	$N(H)$	$N(C^+)$	$N(C)$	$N(CO)$	$N(CH)$	$N(C_2H_2)$	$N(CH_2)$	$N(CCH)$	$N(C_3H_2)^*$
18	5	1E-16	4.6E21	1.4E20	4.9E17	4.7E17	2.5E17	6.3E14	2.5E12	6.8E14	4.0E14	2.4E12
19	5	2E-16	4.6E21	2.2E20	5.1E17	5.0E17	1.9E17	7.4E14	3.5E12	8.5E14	5.0E14	3.1E12
20	3	1E-16	2.8E21	1.1E20	4.8E17	2.0E17	4.6E16	4.2E14	6.6E11	4.2E14	2.4E14	5.0E11
21	3	2E-16	2.7E21	1.6E20	4.8E17	2.0E17	3.6E16	4.4E14	7.0E11	4.5E14	2.6E14	5.2E11

Notes. (*) PDR models do not separate cyclic and linear C_3H_2.

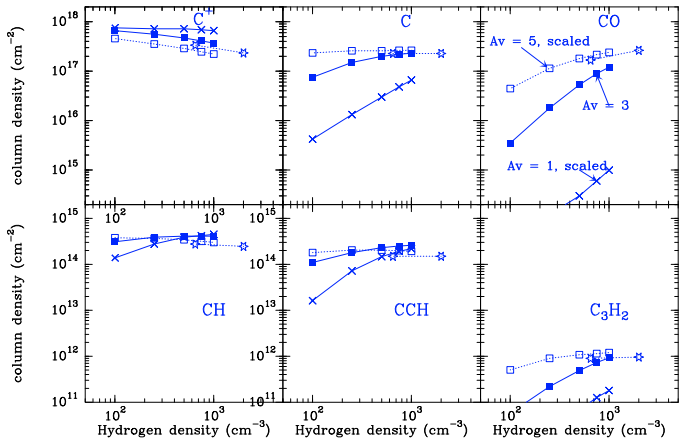

Fig. 5. Prediction of the column densities of C^+, C, CO, CH, CCH and c-C_3H_2 from the PDR Meudon models with various hydrogen densities and pressures. The constant density models are plotted with squares while the constant pressure models are shown with stars. These models correspond to A_V = 3 mag. Results from models with A_V = 5 mag are scaled by 0.6 to compensate for the higher total gas content, they are shown with open squares and dotted lines. Results from models with A_V = 1 mag are scaled by 3 to compensate for the lower total gas content, they are shown with crosses. The constant pressure models are plotted using the highest density point as abscissa.

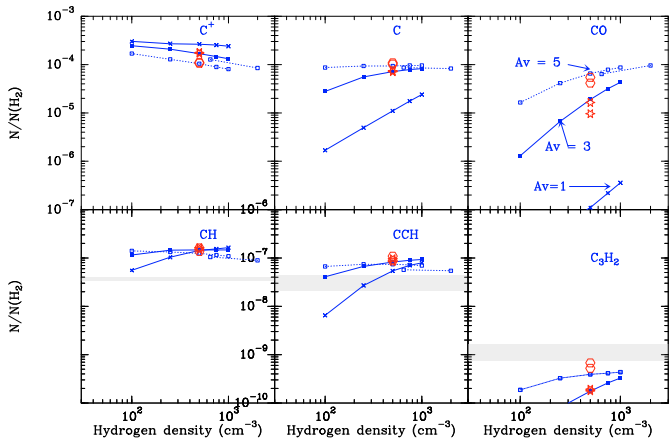

Fig. 6. Prediction of the abundances relative to H_2 of C^+, C, CO, CH, CCH and c-C_3H_2 from the PDR Meudon models with various hydrogen densities and pressures. Models with A_V = 5 mag are plotted with open squares, A_V = 3 mag with black squares and A_V = 1 mag with crosses. Constant pressure models are plotted using the highest density point as abscissa. Models with elevated cosmic ray ionization fluxes are drawn in red, using larger symbols. The gray bars indicate the observed abundances of CH (Sheffer et al. 2008), CCH (Gerin et al. 2010) and c-C_3H_2(this work, using the scaling with CCH).

expected based on the PDR model predictions, that contrasts with the observed tight correlation. In the PDR model, c-C_3H_2 is formed by the dissociative recombination of c-$C_3H_3^+$ and by the reaction of C with acetylene. It is destroyed by photodissociation and by reactions with atomic carbon. It is likely that other formation mechanisms, yet to be identified, participate to the production of c-C_3H_2.

The tight correlation of CCH and c-C_3H_2 was recognized earlier by Lucas & Liszt (2000) and Pety et al. (2005) in different environments (diffuse clouds for the former case and the Horsehead nebula for the latter). The modeling attempts, using an earlier version of the Meudon-PDR code, failed to reproduce this correlation in the context of the Horsehead nebula, a dense molecular cloud illuminated by a moderately intense radiation field (Pety et al. 2005). These authors put forward the hypothesis that the production of c-C_3H_2 and other carbon radicals is increased by the destruction of very small carbon grains and/or PAHs in the intense FUV radiation field at the surface of the molecular cloud, directly exposed to the radiation from

massive stars. In diffuse or translucent clouds, the same mechanism could operate. This scenario needs to be fully tested by including the PAH chemistry in the PDR models.

Godard et al. (2009) have explored the impact of the dissipation of turbulence on the chemistry of diffuse interstellar clouds. They show that the chemical abundances of some molecular species, notably HCO^+ and CH^+, are significantly modified and become in a much better agreement with observations than the predictions obtained by steady-state PDR models. Their chemical network includes CCH but not c-C_3H_2. Models with a more extensive chemical network are currently under investigation, to search whether c-C_3H_2 could be partially produced in the dissipation regions of the interstellar turbulence.

5. Conclusion

We confirm that the tight correlation of CCH and c-C_3H_2 first established by Lucas & Liszt (2000) towards high latitude diffuse clouds is present in the diffuse and translucent matter along the line of sight towards distant massive star forming regions, with $N(\mathrm{CCH}) = (28.2 \pm 1.4) N(\mathrm{c\text{-}C_3H_2})$. This correlation confirms the finding by Lucas & Liszt (2000) and extends it to the more distant interstellar matter in the Galactic Plane. While PDR models seem to reproduce the observed properties of CCH, they fail by at least one order of magnitude for c-C_3H_2. We suggest that CCH might be used as a complementary tracer of molecular hydrogen in diffuse and translucent matter, that can replace CH in environments where no visible spectroscopy can be performed. The HIFI instrument on board the Herschel Space Observatory is now capable of detecting the submillimeter transitions of CH with high accuracy, enabling the direct comparison of CH and CCH.

Acknowledgements. The work was carried out within the framework of the European Associated Laboratory "Astrophysics Poland-France" and also was supported by the Science and High Education Ministry of Poland, grants N203 39/3334. We thank the anonymous referee for her/his very interesting comments that helped to improve the paper.

References

Black, J. H., & Dalgarno, A. 1973, ApL, 15, 79
Cernicharo, J., Cox, P., Fossé, D., & Güsten, R. 1999, A&A, 351, 341
Cox, P., Güsten, R., & Henkel, C. 1988, A&A, 206, 108
Douglas, A. E. 1977, Nature, 269, 130
Falgarone, E., Godard, B., & Cernicharo, J., et al. 2010, A&A, 521, L15
Federman, S. R. 1982, ApJ, 257, 125
Fish, V. L., Reid, M. J., Wilner, D. J., & Churchwell, E. 2003, ApJ, 587, 701
Gerin, M., de Luca, M., Black, J., et al. 2010a, A&A, 518, L110
Gerin, M., De Luca, M., Goicoechea, J. R., et al. 2010b, A&A, 521, L16
Godard, B., Falgarone, E., & Pineau des Forêts, G. 2009, A&A, 495, 847
Godard, B., Falgarone, E., Gerin, M., et al. 2010, A&A, 520, A20
Goicoechea, J. R., & Le Bourlot, J. 2007, A&A, 467, 1
González-García, M., Le Bourlot, J., Le Petit, F., & Roueff, E. 2008, A&A, 485, 127
Herbig, G. H. 1975, ApJ, 196, 129
Herbig, G. H. 1995, ARA&A, 33, 19
Indriolo, N., Geballe, T. R., Oka, T., & McCall, B. J. 2007, ApJ, 671, 1736
Kerr, F. J., & Lynden-Bell, D. 1986, MNRAS, 221, 1023
Koo, Bon-Chul 1997, ApJS, 108, 489
Le Petit, F., Nehmé, C., Le Bourlot, J., & Roueff, E. 2006, ApJS, 64, 506
Liszt, H., & Lucas, R. 2002, A&A, 391, 693
Lucas, R., & Liszt, H. S. 2000, A&A, 358, 1069
Madden, S. C., Irvine, W. M., Swade, D. A., Matthews, H. E., & Friberg, P. 1989, AJ, 97, 1403
Marcelino, N., Cernicharo, J., Agũndez, M., et al. 2007, ApJ, 665, L127
Mul, P. M., & McGowan, J. W. 1980, ApJ, 237, 749
Müller, H. S. P., Thorwirth, S., Roth, D. A., & Winnewisser, W. 2001, A&A, 370, L49
Müller, H. S. P., Schlöder, F., Stutzki, J., & Winnewisser, W. 2005, J. Mol. Struct., 742, 215
Neufeld, D. A., Sonnentrcuker, P., Phillips, T. G., et al. 2010a, A&A, 518, L108
Neufeld, D. A., Goicoechea J. R., Sonnentrucker, P., et al. 2010b, A&A, 521, L10
Padovani, M., Walmsley, C. M., Tafalla, M., Galli, D., & Müller, H. S. P. 2009, A&A, 505, 1199
Penzias, A. A., & Burrus, C. A. 1973, ARA&A, 11, 51
Persson, C., Black, J., Cernicharo, J., et al. 2010, A&A, 521, L45
Pety, J. 2005, in SF2A-2005: Semaine de l'Astrophysique Française, meeting held in Strasbourg, France, ed. F. Casoli, T. Contini, J. M. Hameury, & L. Pagani, (EDP Sciences), Conf. Ser., 721
Pety, J., Teyssier, D., Fossé, D., et al. 2005, A&A, 435, 885
Pickett, H. M., Poynter, R. L., Cohen, E. A., et al. 1998, Submillimeter, Millimeter, and Microwave Spectral Line Catalog, J. Quant. Spectrosc. & Rad. Transfer, 60, 883
Plume, R., Kaufman, M. J., Neufeld, D. A., et al. 2004, ApJ, 605, 247
Roberge, W. G., Jones, D., Lepp, S., & Dalgarno, A. 1991, ApJS, 77, 287
Sakai, N., Saruwatari, O. Sakai, T., Takano, S., & Yamamoto, S. 2010, A&A, 512, 31
Sheffer, Y., Rogers, M., Federman, S. R., et al. 2008, ApJ, 687, 1075
Smith, I. W. M., Herbst, E., & Chang, Q. 2004, MNRAS, 350, 323
Sonnentrucker, P., Neufeld, D. A., Phillips, T. G., et al. 2010, A&A, 521, L12
Teyssier, D., Fossé, D., Gerin, M., et al. 2004, A&A, 417, 135
Thaddeus, P., Guélin, M., & Linke, R. A. 1981, ApJ, 246, L41
Thaddeus, P., Vritlek, J. M., & Gottlieb, C. A. 1985, ApJ, 299, L63
Tielens, A. G. G. M. 2008, ARA&A, 46, 289
Tucker, K. D., Kutner, M. L., & Thaddeus, P. 1974, A&AS, 6, 341
Useli-Bacchitta, F., & Joblin, C. 2007, Molecules in Space and Laboratory, meeting held in Paris, France, May 14–18, ed. J. L. Lemaire, & F. Combes
Vastel, C., Caux, E., Ceccarelli, C., et al. 2000, A&A, 357, 994
Van der Tak, F. F. S., Black, J. H., Schoier, F. L., Jansen, D. J., & van Dishoeck, E. F. 2007, A&A, 468, 627
Weselak, T., Galazutdinov, G. A., Musaev, F. A., & Krelowski, J. 2004, A&A, 414, 949
Williams, J. A., Dickel, H. R., & Rauer, L. H. 2004, ApJS, 153, 463